JOURNAL OF MATERIALS SCIENCE 21 (1986) 2716–2720

Thermal-shock crack patterns explained by single and multiple crack propagation

H.-A. BAHR, G. FISCHER, H.-J. WEISS
Zentralinstitut für Festkörperphysik und Werkstofforschung der Akademie der Wissenschaften der DDR, Dresden and Zentralinstitut für Anorganische Chemie der Akademie der Wissenschaften der DDR, Berlin, German Democratic Republic

The phenomenon of thermal-shock cracking in ceramics is approached theoretically and experimentally. Sintered slabs made from a glass–quartz powder mix were quenched in water in order to generate crack patterns of various types, depending on the severity of the shock. The patterns serve as evidence for a scheme set up with the aim of explaining the variety of ways in which materials respond to thermal shock. The fracture-mechanical explanations are based on the time-dependent thermal load and on the concept of an energy release rate, with single and multiple crack propagation starting from randomly distributed initial flaws on the surface.

1. Introduction

The formation of thermal-shock crack patterns can be appropriately discussed in terms of fracture mechanics, whose central notion is a crack propagation criterion expressed by the stress intensity K_I or the energy release rate $\mathcal{G}$.

The implications of time-dependent $\mathcal{G}$ curves for single crack propagation due to thermal shock have been anticipated but not thoroughly worked out by several authors. Kerkhof and co-workers [1, 2] calculated the stress intensity factor K_I, which is related to $\mathcal{G}$ in a simple way, of notched slabs with ideal cooling on one face. The corresponding problem for cylinders with multiple radial notches was discussed by Evans and Charles [3]. Emery and Kobayashi [4] calculated K_I for rectangular bars subjected to thermal shock on all side faces.

This paper is composed according to the following scheme. First, we present thermal-shock crack patterns obtained by the quenching of ceramic slabs. Second, we try to explain the patterns by unstable and stable crack propagation governed by time-dependent $\mathcal{G}$ curves, taking into account the results by Nemat-Nasser *et al.* [5] and Bazant *et al.* [6] on the mutual interaction of cracks. In view of the nature of the problem we chose not to formulate it mathematically but preferred to derive our results along the lines of physical reasoning aided by graphical representations, the latter incorporating essential features of the exact solutions. Thus, most of the mathematics involved is left hidden in the plots, and attention is focused on conclusions, results, and implications in verbal form. For conciseness we refer to a publication [7] where some auxiliary ideas have been outlined in more detail. The experimental procedure is a modified version of that used by Davidge and Tappin [8].

2. Experimental procedure

Quartz and glass powders (median grain size 5.8 and 2.9 μm, respectively) were dry-mixed, then wet-mixed after the addition of auxiliary substances and spray-dried. The granulate containing 10 vol % quartz was pressed at 100 MPa into slabs of size 5 mm × 10 mm × 60 mm and subsequently sintered without pressure. The porosity after sintering was 4%. The samples were ground to obtain smooth parallel faces, then stacked as seen in Fig. 1 in order to prevent access of the coolant to the side faces. The stacks were heated in an alumina tube and from there immediately dropped into water at room temperature. After drying, the samples were covered with a fluorescent liquid for 5 min and then washed in water and acetone. The liquid still present within the cracks was made to fluoresce by ultraviolet light.

The crack patterns thus made visible were photographed by using a special filter. Four faces of every sample are shown in Fig. 2. The photographs have been arranged so that the cracks on the side faces, which mainly concern us here, can be easily related to those on the cooled surface.

With increasing severity of shock the stress changes from mainly uniaxial to mainly plane, as seen from the net-like surface crack patterns. Our samples were given the shape of slabs with the narrow faces cooled, with the intention of approaching uniaxial stress in the cooled layer, at least with lower ΔT values where crack propagation occurs when the cooling has penetrated deep into the sample. (For explanation see Section 4.) The purpose was to obtain simple crack patterns which exhibit no additional structure in the third dimension. Indeed our samples show patterns that are mainly simple in this sense, up to moderate shocking temperatures (Figs 2a and b).

Evidently the crack density increases with severity of shock. Furthermore, there are subtle features hidden in the patterns whose significance may not be self-evident at first sight: At higher ΔT, there is a tendency to the ordering of cracks with respect to

0022–2461/86 $03.00 + .12

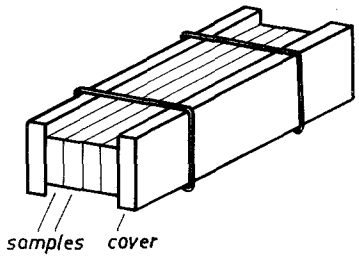

Figure 1 Stack of samples prepared for thermal shocking.

length and spacing. There is a tendency to form a kink in the crack path at a certain depth which decreases with increasing ΔT (see arrows in Fig. 2). These features play an essential part in the following considerations.

3. Crack penetration history

Thermal shocking gives rise to tensile stress within the cooled layer. The stress is largest at the surface and decays with depth. A qualitative understanding can be reached without knowing the thermal stress field exactly. As we intend to discuss cracking as a two-dimensional phenomenon observable on the side faces of samples of small thickness, we will not worry at present about what is going on in the third dimension. The formation of surface crack patterns is considered later.

The crack patterns as they appear on the side faces suggest that they have been formed in at least two steps. So understanding the crack patterns requires understanding their history, which can be achieved by considering time-dependent energy release rates.

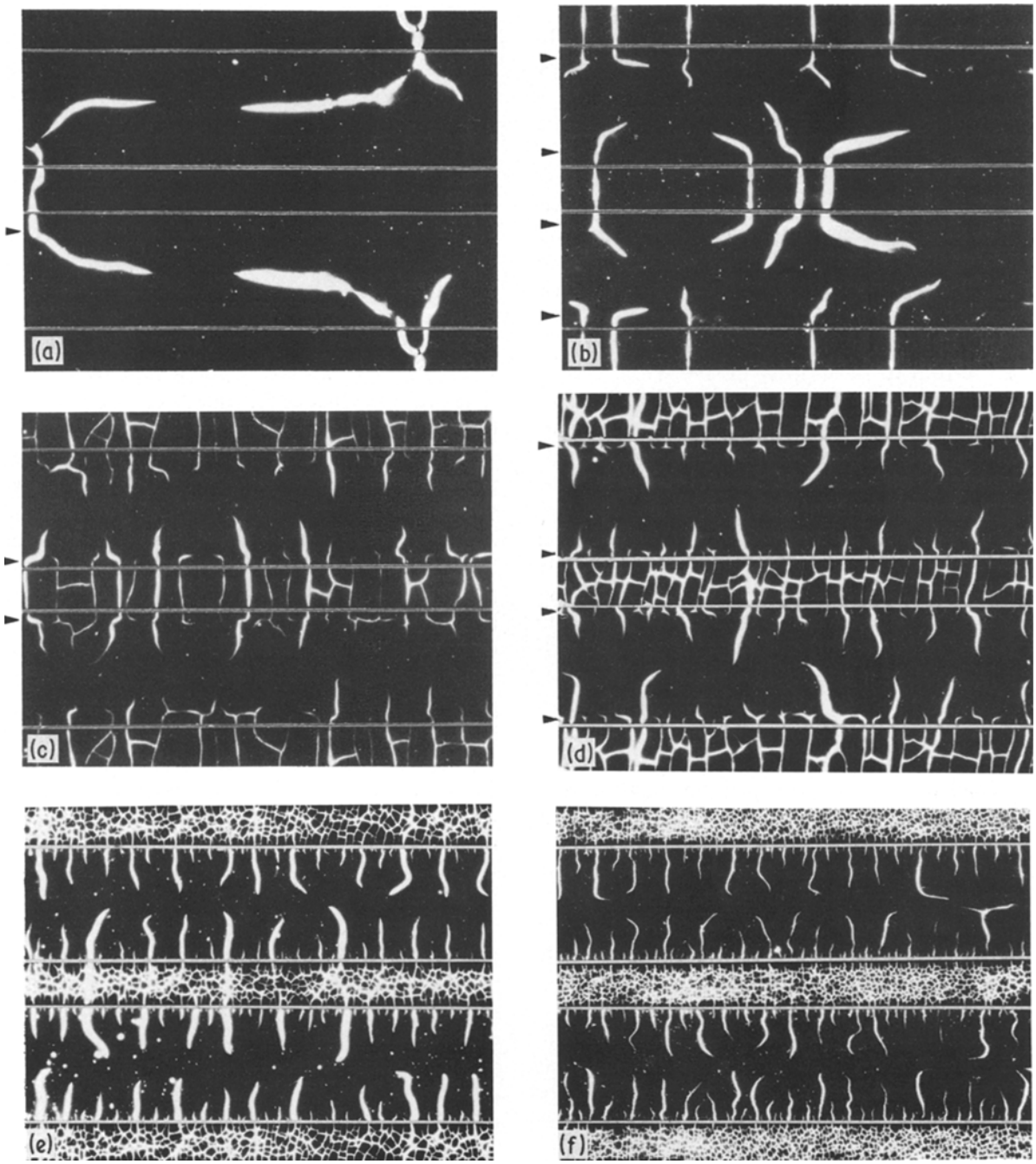

Figure 2 Thermal shock crack patterns made visible by fluorescent liquid on side faces (wide strips) and cooled surface (narrow strips). Only part of every sample is shown. Arrows indicate supposed depth of unstable cracking. ΔT = (a) 159, (b) 181, (c) 217, (d) 233, (e) 300, (f) 340 K.

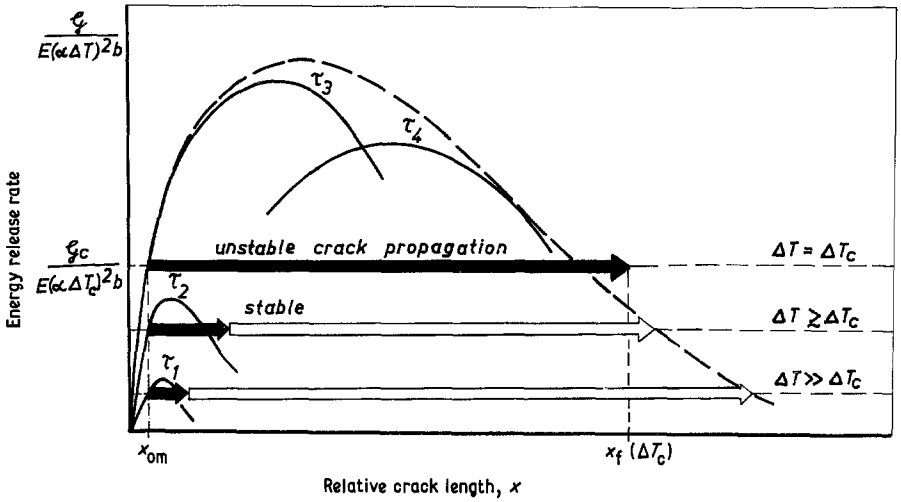

Figure 3 Relation between energy release rate $\mathcal{G}$ and crack length (schematic). (—) Family of curves generated by time dependence, and (– – –) their envelope, which is essential for crack propagation. Arrows refer to final crack lengths for three arbitrarily chosen values of the temperature difference in quenching, ΔT. Solid and open arrows refer to unstable and stable propagation, respectively; x = ratio between crack length and sample dimension b, α = thermal expansion coefficient, E = Young's modulus, $\tau = \kappa t/b^2$ = normalized time, κ = thermal diffusivity.

Information concerning the latter can be obtained by physical reasoning as explained in the Appendix. With the crack propagation criterion $\mathcal{G} \geqslant \mathcal{G}_c$ and the family of $\mathcal{G}$ curves in Fig. 3, essential features of the crack history can be derived.

In order to explain the observed crack patterns we proceed as follows. We derive possible crack histories from the schematic $\mathcal{G}$ curves and substantiate them by experimental evidence. In doing so we distinguish two cases with respect to severity of shock: first, shocking slightly above the threshold below which there is no cracking, $\Delta T \gtrsim \Delta T_c$, and, second, shocking well above that threshold, $\Delta T \gg \Delta T_c$.

3.1. ΔT equal to or slightly above ΔT_c

At the threshold of cracking, at $\Delta T = \Delta T_c$, the temperature difference in quenching is just high enough to activate the largest of the small pre-existing cracks, whose relative length (i.e. length with respect to sample size) is denoted by x_{om}, where $x_{om} \ll 1$. In Fig. 3, cracks of length x_{om} start to propagate at the (normalized) time τ_3 when $\mathcal{G}(x_{om})$ reaches $\mathcal{G}_c$. This condition can be reformulated in the way that the envelope of the family of $\mathcal{G}$ curves must intersect the horizontal straight line representing $\mathcal{G}_c$ at x_{om}. Since this occurs always on the upward slope of the curve, $\mathcal{G}$ increases with crack propagation, which implies unstable propagation. (In our figures, unstable propagation is always indicated by solid arrows.) How far the crack moves unstably depends on how much of the excess energy released (i.e. $\mathcal{G} - \mathcal{G}_c$ accumulated along the crack path) is re-absorbed by the running crack tip after $\mathcal{G}$ has dropped below $\mathcal{G}_c$. There is experimental evidence [9, 10] that the excess released energy is not dissipated immediately; Fig. 3 refers to materials with very small x_{om}, which means high strength, where unstable cracking may overshoot the envelope.

Increasing ΔT above ΔT_c means lowering the horizontal line representing $\mathcal{G}_c$ in Fig. 3, as a consequence of our normalized representation. So the initial cracks of relative length x_{om} start a bit earlier (at τ_2, for instance). They quickly overshoot the slowly changing $\mathcal{G}$ curve and then stop. As $\mathcal{G}$ is still increasing, smaller initial flaws are activated in addition to the largest ones. The stopped cracks move on after a while when their $\mathcal{G}$ exceeds $\mathcal{G}_c$ again, being pushed along stably as the intersection point between the downward part of the $\mathcal{G}$ curve and the $\mathcal{G}_c$ line moves to the right until it touches the envelope. Thus the final crack length $x_f(\Delta T)$ is determined by the envelope of the family of $\mathcal{G}$ curves.

If ΔT is chosen only slightly above ΔT_c, the mutual separations of cracks are much larger than their lengths, so that crack start and propagation are essentially governed by the $\mathcal{G}$ curves of single-crack propagation. The smallest crack to be started is determined by the envelope again, and thus is only a little smaller than x_{om}.

3.2. ΔT well above ΔT_c

With larger ΔT, unstable cracking is partly suppressed in favour of subsequent stable crack growth, as seen from Fig. 3. Also with increased severity of shock, cracks start at ever shorter times when the cooling has penetrated into smaller depths, as explained above. As a consequence, unstable crack paths become shorter. The higher the value of ΔT, the smaller are the initial flaws that can be induced to grow into cracks. Since the smaller flaws usually outnumber the larger ones, the resulting cracks become more closely spaced. The unloading of the vicinity of every crack puts a limit to the crack density. Thus the average spacing of unstably grown cracks is expected to be roughly equal to their length. A tendency to this kind of order is found in Figs 2c and d, and is probably present also at higher ΔT but not clearly visible there because of the smallness of the distances. (The unstably traversed part of the crack paths supposedly shows up in the patterns, as explained in Section 4, and indicated by arrows in Fig. 2.)

As the cooling penetrates further in depth, subsequent stable crack growth is governed by progressive mutual unloading. Thus the $\mathcal{G}$ curves of Fig. 3, representing single cracks, do not apply any more. Not all cracks once started can be kept propagating: roughly speaking, every second crack is left behind. This will occur repeatedly every time the remaining cracks have grown to lengths competing with their lateral separations, forming in this way a hierarchical order of cracks. The phenomenon has been predicted theoretically for highly symmetrical situations [5, 6], and verified experimentally by Geyer and Nemat-Nasser [11] with notched glass plates. In reality, of course, the

regularity is partly spoiled by random influences of various origins. Surprisingly, the hierarchical order sometimes stands out clearly against the random background, as seen on our quenched ceramic slabs. (See, for instance, Fig. 2f, top right-hand region. Note that our samples have not been artificially notched.) The mechanism explained above seems to have been at work in the one unnotched glass plate shown in the paper by Geyer and Nemat-Nasser [11] in their Fig. 2.

4. Observational details

Let us look at our samples for more of the phenomena predicted above. As sparse cracking is observed at $\Delta T = 159\,\mathrm{K}$ while at 154 K there is no cracking at all, ΔT_c must be situated between these values. A comprehensive view of the side faces of the samples reveals the existence of a characteristic length affecting the shape of the cracks independent of their lengths: it is the short distance from the sample surface to the first bend in the crack path. It is largest at small ΔT and decreases with increasing ΔT (see arrows in Fig. 2). This suggests that the characteristic length visible in the crack patterns is equivalent to the final length of unstable propagation of hypothetical straight cracks. We adopt this view henceforth, and justify it by the following explanation. A straight crack would be trapped at some depth where $\mathcal{G}$ is low. The real crack, however, evades being trapped by changing to a spalling mode of propagation which still offers sufficient energy release, and then stops half-way.

Luckily we need not consider the intricate problem of curved cracks in detail; the experimental fact that, after the kinks, the cracks move on in depth, at least at higher ΔT, seems to indicate that further growth is not much affected by the existence of the kink in the path. Near the mid-plane of the sample, long cracks, too, tend to turn to spalling, for similar reasons as the short ones did.

After having tried to explain the crack patterns visible on the side faces of the samples, let us turn to the patterns appearing on the cooled surface. At low ΔT they provide nothing new in addition to the structure seen on the side face. In order to explain their changing appearance with increasing ΔT, we consider the other extreme, which is cracking of a thin layer at high ΔT. If the cooled layer is thin compared with the thickness of the slab, the type of thermal stress is isotropic plane stress. Therefore the cracks form a network with no preferred direction. This kind of isotropy, of course, is not necessarily related to high ΔT; it would also appear at lower ΔT if the quenched body was bulky enough.

The dependence of the crack density on ΔT has been explained already for the patterns on the side faces. For completeness it should be mentioned that the patterns provide still more information. As a striking feature of Figs 2a to d, cracks on the cooled surface run preferentially straight between the edges, and parallel to each other. At the time when the surface crack pattern forms, the depth to which the cooling has penetrated is smaller than the width of the sample, as seen from the positions of the kinks in the crack paths on the side faces (indicated by arrows). So one has to conclude that thermal stress on the cooled face is more plane than uniaxial at the moment of crack formation; one would then expect a tendency towards isotropy in the patterns at lower ΔT, too, and the significantly different appearance of the patterns requires an explanation. It seems that in Fig. 2, cracking is dominated by edge flaws. As stress is uniaxial along the edge, cracks starting there move perpendicular to the edge, which explains the nearly parallel straight cracks prevailing in the patterns, especially at lower ΔT. At higher ΔT, plane stress reveals itself by the net-like character appearing in the patterns some distance away from the edge.

5. Concluding remarks

It has been shown that all the essential features of crack patterns appearing on quenched samples can be understood by considering single and multiple crack propagation in thermal stress fields changing with time. It seems that the findings do not much depend on whether thermal stress is predominantly uniaxial or plane. Thus it may be justified to regard our results not as pertaining to a special kind of sample but to quenched bodies in general.

Since the strength retained after shocking depends on the length of cracks present within the shocked material, a better understanding of thermal shock damage, especially strength degradation, may be reached by considering the final crack lengths forming in thermal shock. Explanations given in the literature are based on the pioneering work of Hasselman [12], whose model seems to be of remarkable but nevertheless limited power in so far as it does not consider the build-up of thermal stress in the course of time. This is the reason why we devoted this paper to the understanding of crack patterns. Thermal shock damage as seen from this vantage point will be the subject of a forthcoming paper [13].

Appendix: Time-dependent $\mathcal{G}$ curves and cracking in thermal shock

The cracking of brittle materials is usually understood in the following way. Initial flaws or notches within a loaded body can be characterized by the amount of energy which they would release when extending their size by an incremental cut. The energy per cut area released in this way is called the energy release rate $\mathcal{G}$. As soon as $\mathcal{G}$ for a given flaw, notch or pre-existing crack surpasses a critical value $\mathcal{G}_c$ in the course of time,

$$\mathcal{G} \geqslant \mathcal{G}_c$$

crack propagation starts and continues as long as this condition is met. It is well known that $\mathcal{G}_c$ may also depend on crack length or on loading rate more or less significantly. It seems, however, that the assumption of constant $\mathcal{G}_c$ approaches reality sufficiently well in our experiments.

$\mathcal{G}$ depends on the size, shape, position and orientation of the crack within the body. However, we follow the common practice of considering only cracks of such a kind and positioned in such a way that they are adequately described by only one parameter, namely the crack length.

$\mathcal{G}$ is proportional to the square of the stress which would be present within the body in the absence of the crack. Since in our problem the load is of thermal origin, where the temperature field is non-stationary, $\mathcal{G}$ changes with time t. The variables involved enter into the formalism as dimensionless combinations, namely relative crack length $l/b \equiv x$, reduced time $\kappa t/b^2 \equiv \tau$ and Biot modulus $hb/k \equiv \beta$, where l, b, κ, h and k denote crack length, body diameter, thermal diffusivity, heat transition and thermal conductivity, respectively. For reasons of dimensionality, $\mathcal{G}$ may then be written [1–4, 7] as

$$\mathcal{G} = Eb(\alpha\Delta T)^2 f(x, \tau, \beta)$$

where ΔT is the temperature difference between the sample before cooling and the coolant, α is the thermal coefficient and E is Young's modulus. Dimensionless factors containing Poisson's ratio, which do not anyway much differ from unity, are omitted here.

This suggests that one should plot not $\mathcal{G}$ but $f(x, \tau, \beta)$ against x, with the advantage that any quenching temperature can be discussed with the same plot of curves. We chose to plot families of curves generated by the parameter τ (Fig. 3).

We emphasize that the essential features of time-dependent $\mathcal{G}$ curves can be deduced by physical reasoning. This enables us, for instance, to extrapolate the numerical results from the literature, which are not always given within the whole region of interest. In the range of small crack lengths corresponding to natural flaws, the published numerical results seem to be of low accuracy so that delicate features of the curves do not show up there. In this paper we do not keep to those numerical results obtained for special sample shapes, but prefer plotting schematical $\mathcal{G}$ curves instead which are more suitable for explaining things.

The overall shape of the curves is mainly determined by both the initial slope and the fact that $\mathcal{G}$ tends towards zero for long cracks where the crack tip is located deep below the quenched layer.

In the general case of finite Biot modulus β the temperature on the cooled surface changes gradually and approaches that of the coolant asymptotically. Thus, tensile stress and $\partial\mathcal{G}/\partial x$ increase with time. At large times, the situation is characterized by the decay of thermal stresses as the temperature gradually levels out: the curves become flatter and finally degenerate into the abscissa axis.

Note that there is an envelope to the family of $\mathcal{G}$ curves. This envelope is essential for explaining crack propagation.

References

1. J. G. BLAUEL and F. KERKHOF, *Chemie-Ing.-Techn.* **43** (1971) 746.
2. D. STAHN and F. KERKHOF, *Glastechn. Ber.* **50** (1977) 121.
3. A. G. EVANS and E. A. CHARLES, *J. Amer. Ceram. Soc.* **60** (1977) 22.
4. A. F. EMERY and A. S. KOBAYASHI, *ibid.* **63** (1980) 410.
5. S. NEMAT-NASSER, L. M. KEER and K. S. PARIHAR, *Int. J. Solid Struct.* **14** (1978) 409.
6. Z. P. BAZANT, H. OHTSUBA and K. AOH, *Int. J. Fract.* **15** (1979) 443.
7. H.-A. BAHR and H.-J. WEISS, in "Current Topics in Materials Science", Vol. 12, edited by E. Kaldis (North-Holland, Amsterdam, 1985) Ch. 4, Sect. 4.
8. R. W. DAVIDGE and G. TAPPIN, *Trans. Br. Ceram. Soc.* **66** (1967) 405.
9. A. G. EVANS, *Proc. Br. Ceram. Soc.* **25** (1975) 217.
10. C. SCHUBERT, H.-A. BAHR and H.-J. WEISS, *Carbon* **24** (1986) 24.
11. J. F. GEYER and S. NEMAT-NASSER, *Int. J. Solid Struct.* **18** (1982) 349.
12. D. P. H. HASSELMAN, *J. Amer. Ceram. Soc.* **52** (1969) 600.
13. H.-A. BAHR and H.-J. WEISS, *Theor. Appl. Fract. Mech.*, in press.

Received 12 June
and accepted 26 September 1985